Bulletin of the Seismological Society of America, in press, 2002

Slip distribution of the September 7, 1999 Athens earthquake inferred from an empirical Green's function study

by Z. Roumelioti[1], D. Dreger[2], A. Kiratzi[1] and N. Theodoulidis[3]

[1] Department of Geophysics, Aristotle University of Thessaloniki, P.O. Box 352-1, 54006 Thessaloniki, Greece
[2] Berkeley Seismological Laboratory, University of California, 281 McCone Hall, Berkeley, CA 94720
[3] Institute of Engineering Seismology and Earthquake Engineering, P.O. Box 53, 55102, Thessaloniki, Greece

Abstract The source process during the September 7, 1999 Athens (Greece) earthquake is investigated using broadband seismograms recorded at regional distances. Source time functions are estimated through an empirical Green's function approach and their shapes are inverted to reveal the spatial and temporal distribution of fault slip. The resulting slip distribution pattern implies that around 50% of the total slip occurred at depth greater than the hypocentral depth, indicating downward rupture propagation, while 25% of the total slip was concentrated at a shallower patch. Forward calculations of the displacement field at the surface show that the shallower slip patch is possibly responsible for the asymmetry observed in the displacement field and it may have contributed significantly to the distribution of damage.

Introduction

On September 7, 1999 a moderate size earthquake (**M** 5.9) occurred within a few kilometers from the center of the metropolitan city of Athens, the capital of Greece. Despite its moderate size, the earthquake caused extensive damage, mainly concentrated at the N-NW suburbs of the city. 143 people were killed

in 30 collapsed buildings, both residential and industrial, while reported injuries were as high as 2,000 (Anastasiadis et al., 1999; Papadopoulos et al., 2000; Gazetas, 2001).

Although the earthquake triggered 15 accelerographs within 30 Km from the epicenter, none of these instruments was installed within the meizoseismal area. Therefore, the actual strong ground motions in this area are only inferred from the distribution of the damage or other phenomena like the toppling of heavy cemetery monuments (Gazetas, 2001).

High levels of excitation, which can be attributed to several factors, can only explain the extensive damage reported in the N-NW part of Athens. Among these factors, local soil conditions and topographic relief are believed to have significantly contributed to the intensity and the geographical distribution of damage (Anastasiadis et al., 1999; Marinos et al., 1999; Gazetas, 2001; Bouckovalas and Kouretzis, 2001). Furthermore, synthetic calculations of strong ground motion imply the occurrence of directivity effects towards the heavily affected area (Tselentis and Zahradnik, 2000; Roumelioti et al., 2002; Zahradnik and Tselentis, 2002).

In the present work we examine the contribution of the seismic source to the damage distribution pattern of the Athens earthquake. In particular, we investigate the source process during the Athens mainshock, using a method of earthquake source inversion introduced by Mori and Hartzell (1990) for

local earthquakes and extended to regional distances by Dreger (1994). The applied method involves estimation of the source time functions (STF) of the mainshock by deconvolving broadband body waves from a nearby smaller event with similar focal mechanism (empirical Green's function). The resulted STF's are back - propagated onto the fault plane to produce an estimate of the slip distribution and kinematic parameters of the rupture.

Data

The data used consist of broadband waveforms recorded by the Greek national broadband network, operated by the National Observatory of Athens (NOA). The stations of the network are equipped with Lennartz LE-3D/20s sensors. At the time of the examined event, only the two horizontal components were recorded by these sensors, while the vertical component was recorded only by short period sensors and was therefore not used in our study. The above data were supplemented by data from station SER, which is jointly operated by Charles University and the University of Patras. This station is equipped with a Guralp CMG-3T sensor and provided the closest broadband waveforms of the Athens earthquake.

The azimuthal distribution of the stations used in this study, with regard to the epicenter of the examined event, is shown in Figure 1. In general, the station coverage has a large bearing on the applicability of the method and especially on the ability to determine the relative amplitudes of different subevents

(Antolik, 1996). In the case of the Athens mainshock, the station coverage is satisfactorily good, since the largest azimuthal gap is around 60 degrees.

Methodology

In the frequency domain and in the case of a point source, the far-field wave displacement, $U(\omega)$ recorded at distance r and azimuth ϕ can be represented by:

$$U(\omega) = \dot{M}(\omega) \cdot G(\omega, r, \phi) \cdot R \cdot I(\omega) \quad (1)$$

where $\dot{M}$ is the moment rate function (source time function) of the event, G is the Green's function response of the medium along the wave path, which includes the effects of attenuation and geometrical spreading, R is the radiation pattern factor and I is the response of the recording instrument. In order to retrieve the desired source time functions from the displacement records one has to remove the effects of the propagation path and the recording instrument. A simple way to accomplish this is by deconvolving the waveforms of a nearby smaller event with similar focal mechanism, herein referred to as an empirical Green's function (eGf). In this approach the small event is assumed to be a point source in both time and space and to the extent that this assumption does not hold the STF of the target event will be a relative estimate to the STF of the small event. Therefore, the eGf should be small enough to be treated as a point source, but also large enough to ensure a satisfactory signal to noise level at the examined distances.

In the following stage and prior to the inversion, the estimated STF's are normalized to unit area. This is done to avoid problems with amplitudes due to differences in the radiation patterns of the eGf and mainshock, and to ensure that all of the STFs used integrate to the appropriate scalar seismic moment. This also tends to equalize the weighting of individual STFs in the inversion. The following step involves the inversion of the STF's, which are estimated as described previously. The employed inversion technique (Mori and Hartzell, 1990) is based on the assumption that the variations in STF shape can be mapped onto the spatial and temporal slip history of the event. The source is parameterized through a radially propagating rupture front, which expands with a constant rupture velocity. Slip is confined to one of the nodal planes indicated by the focal mechanism of the event. Then the inverse method fits the STF of the examined event by summing contributions from different subfaults, taking into account the time delay due to wave propagation and to the propagation of the rupture front, with respect to the hypocenter. Distances to the different subfaults are estimated using a half space ray trajectory approximation. The contribution from each subfault can take the form of several synthetic time functions. Here the subfault STF's have the form of boxcar functions. The optimal values for the fault orientation, the rupture velocity and the dislocation rise time are found by performing a series of inversions testing the parameter space.

The subfault STF's (B) are related to the observed STF's (D) through a system of equations of the form:

$$D_i(t) = STF_i(t) = \sum_j^m B_j(t-\tau_{ij})w_j \quad (2)$$

where τ is the time delay due to wave and rupture propagation, i is a station index, j is a subfault index and w is a weight proportional to fault slip. In the above system of equations we also impose a positivity constraint to require all subfaults to have the same slip direction. A spatial derivative minimization constraint is applied to smooth the resulting slip model. As a result, equation (2) can finally be written in matrix form as:

$$\left[\frac{\mathbf{B}}{\lambda\mathbf{S}}\right] \cdot w = \left[\frac{\mathbf{D}}{0}\right] \quad (3)$$

where **S** is the matrix of first spatial derivatives and λ is a constant controlling the weight of the smoothing equation.

The slip weight vector is obtained by standard least squares. Slip amplitudes at each subfault, u_j, are finally obtained based on an independent seismic moment estimate, M_0, through the relation:

$$u_j = \frac{M_0 \cdot w_j}{A \cdot \mu} \quad (4)$$

where A is the subfault area and μ is the shear modulus, usually taken equal to 3.5×10^{10} Pa.

Application

The choice of the appropriate STF in the study of the Athens mainshock was based on the published focal mechanisms (Papadimitriou et al., 2000; Papadopoulos et al., 2000; Papazachos et al., 2001; Louvari and Kiratzi,

2001; Zahradnik, 2002) and additionally on the direct comparison of the mainshock waveforms to the waveforms of the largest aftershocks. An aftershock of **M** 4.5 was identified as suitable for our study. The parameters of this aftershock are presented in Table 1, along with the parameters estimated for the mainshock from several authors. In Figure 2 we compare the horizontal displacement seismograms at three different stations for the mainshock and the chosen aftershock. Even though the waveforms of both the small and large event show considerable complexity along the different regional paths, the aftershock seems to be satisfactorily identical to the target event within the examined frequency range.

The source time functions of the Athens mainshock were estimated using the broadband waveforms from the stations depicted in Figure 1. The original broadband data were integrated to displacement and band pass filtered in the frequency range 0.05 Hz – 1.0 Hz. A 1% water-level (Clayton and Wiggins, 1976) was used to stabilize the deconvolution process. In order to enhance the quality of the output, in most stations we independently used each one of the two horizontal components and stacked the resulting source time functions. In this way, the required STF is better enhanced through a reduction of the background noise level. An example of the stacking procedure at one of the examined stations (APE) is depicted in Figure 3.

The resulting STF, normalized to unit area, for each of the nine stations used are shown in Figure 4. The distinctive differences among the shapes and

amplitudes of the STF allow us to draw some first conclusions in respect to the emergence of directivity effects. Source time functions at E-SE (e.g. stations APE, ARG, PRK) present larger amplitudes and shorter durations (2-3 sec), which indicate propagation of the rupture towards this direction. On the contrary, STF estimated at W-NW stations (e.g. KZN, JAN, SER etc.) present considerably lower amplitudes and durations as long as 4-5 sec.

For the inversion of the STF shapes we employed a planar fault model of 25x25 Km discretized into 1 Km^2 square subfaults. The dimensions were chosen to be larger than those expected for an **M** 5.9 earthquake to avoid errors at the boundaries of our model. The fault plane was oriented relatively to the hypocenter at a depth of 8 Km (Papadimitriou et al., 2000). Nevertheless, we ought to mention that significant discrepancy exists among the published epicentral coordinates and focal depths (Papadopoulos et al., 2000; Papazachos et al., 2001; Papadimitriou et al., 2000; USGS) and therefore our results are subject to the error included in the employed location. In more detail, the proposed epicentral locations differ from each other from 3 to 16 Km, while the hypocentral depth ranges from 8 to 17 Km. However, this uncertainty affects the absolute location of slip and not its hypocenter-relative position. This is due to the fact that the examined stations are located at regional distances and therefore the differences in the hypocenter parameters are not large enough to alter their relative position with respect to the fault plane.

Although the rupture velocity and the dislocation rise time are fixed during the inversion procedure, several values were tested to reveal the optimum combination. The values examined lie within the range from 0.1 to 1.0 sec for the dislocation rise time and from 1.6 to 3.4 Km/sec for the rupture velocity. Although the applied methodology, as has been shown repeatedly for other events, is able to identify the causative fault plane from the two possible nodal planes, as well as the rise time and rupture velocity, for the Athens event the magnitude is relatively small and therefore the source dimensions do not allow a clear distinction. We were only able to identify a shallow minimum in variance for a rise time of 0.4 sec and a rupture velocity of 2.5 to 2.7 Km/sec. The slip weights, derived from the STF inversion, were scaled based on the value of seismic moment (M_0=9.22×10^{17} Nm) estimated by Louvari and Kiratzi (2001) and the resulting slip distribution pattern is presented in Figure 5. The activated area is confined to a 10x10 Km region of the modeled fault surface, while the rupture seems to have stopped at a depth of ~5 Km below the ground surface. This partly explains the absence of clear surface ruptures (Pavlides et al., 2002) and is in good agreement with the results from studies regarding the aftershock distribution (e.g. Papazachos et al., 2001). The average slip across the part of the fault model that ruptured is around 16 cm, a value which is consistent with the values estimated from empirical relationships applicable to Greece or globally (e.g. Papazachos and Papazachou, 1997; Wells and Coppersmith, 1994) and close to the value determined by spectral analysis of teleseismic data (Louvari and Kiratzi,

2001). Locally the slip appears to be significantly larger and the peak value (~95 cm) is observed very close to the hypocenter location.

Generally, the slip appears to be concentrated in two patches. The prevailing slip patch concentrates around 50% of the total slip and is located at a depth greater than the hypocentral depth, indicating downward propagation. Another 25% of the total slip appears at shallower depths (~5-8 Km, taking into account the fault dip) and indicates a strong directivity towards E-SE. Although damage is usually associated with areas of high ground velocity or acceleration, this observation might be of great significance, since most of the severely affected areas were reported close to the east edge of the fault. The rest, 25% of the total slip, appears as areas of very low levels of slip around the two main patches.

Forward modeling to calculate the displacement field

The estimated slip pattern was tested in terms of its capability of explaining the distribution of damage during the Athens mainshock. This test was performed through forward calculations of the displacement field at the surface and comparison of the resulting pattern with the displacement field estimated from interferometric data by Kontoes et al. (2000). The forward calculations were performed using the code of Kaverina et al. (2002), which includes subroutines by Okada (1985).

We performed three calculations of the displacement field at the surface by successively examining the effect of the entire slip model and the contributions of the shallower slip patch and the deep slip patch in the overall field. The resulting displacement maps are shown in Figure 6, along with the interferogram of Kontoes et al. (2000), which is shown for comparison. In the latter work, two concentric fringes, corresponding to 56 mm in slant range, were observed in the meizoseismal area. The two fringes present an asymmetry at the E-SE of the affected area, where most of the damage was reported. As can be seen in Figure 6b, the synthetic displacement field deduced from the estimated slip distribution model also shows an asymmetry towards this direction. This anomaly is connected to the shallower slip patch (Figure 6c), since the deep slip patch results in a perfectly symmetric displacement field at the surface (Figure 6d). The absolute values of the synthetic displacements are also in good agreement with the results of Kontoes et al. (2000), although this greatly depends on the employed value of the scalar seismic moment, which is used to scale the subfault slip.

Conclusions – Discussion

We present results of the source process during the 1999 Athens earthquake and the effect that this process had on the distribution of damage. The source was investigated through a source time function inversion technique, which revealed a concentration of slip in two patches. Most of the slip (~50% of the total slip) occurred at depth greater than the hypocentral depth, while a significant amount (25%) was concentrated at a shallower patch, which

nevertheless did not reach the surface. The activated area was confined to about 100 Km^2 and a maximum variance reduction between the synthetic and the observed STF was obtained for a rise time of 0.4 sec and a rupture velocity close to 2.7 Km/sec.

The credibility of the estimated slip model was tested through forward calculations of the surface displacement field and comparison of the results with interferometric data. The asymmetry in the observed displacement field (Kontoes et al. 2000), which is connected to the irregular distribution of damage in the epicentral area, was successfully reproduced in the synthetic field. Taking into account the inability of the employed methodology to reveal small-scale characteristics of the slip history, the reproduction of the anomaly in the shape of the simulated displacement field is supportive of the intensity of the modeled directivity effects towards E-SE.

The investigation of the contribution of each one of the two prevailing slip patches to the overall surface displacement field revealed that the shallower slip patch is probably responsible for the asymmetric deformation of the affected area. The channeling of the energy towards east can be attributed to the morphological characteristics of the area (Papazachos et al., 2001; Gazetas, 2001). In particular, our results confirm the assumption that the Aegaleo Mountain range at the SE of the activated area may have acted as a geometric barrier to the downward propagation of the rupture at the eastern part of the seismogenic fault. This might have caused a confinement of the

slip at shallower depths, which acted catastrophically at the E-NE part of the deformed area.

On the other hand, most of the seismic energy was released uniformly, within a much larger area, as a result of the downward propagation of the rupture in the deep-slip patch. The downward propagation of the rupture is of great interest as other studies related to the Athens earthquake, imply upward propagation (Papadopoulos et al., 2000; Papazachos et al., 2001). Their assumption is basically related to the depth of the mainshock hypocenter, which appears to be below the zone of aftershock concentration. Our attempts to estimate the slip model based on larger depth values (compared to the finally employed value of 8 Km) resulted in a dislocation of the entire model to greater depths, without significant changes in the slip-hypocenter relative position. In these models, most of the slip appeared at unrealistically large depths (20-25 Km), compared to what is commonly believed for Greek earthquakes (Papazachos and Papazachou, 1997). Furthermore, the corresponding synthetic surface displacement fields were also shifted towards south, deviating from the interferometric observations. These results comprised our basic restrictions regarding the choice of the finally used value for the hypocentral depth.

In conclusion, the 1999 Athens mainshock can be regarded as another demonstration of the impact that the source process can have in the near field of a seismogenic fault, even in cases of moderate magnitude earthquakes.

Such events impose the need of a deterministic inclusion of the seismic source in the simulation of future strong ground motions. However, we should not ignore our incapability of predicting the behavior of a seismogenic fault in a future earthquake and therefore the difficulty in deterministically modeling the slip distribution of a future event. Recent attempts to identify systematic features of slip models for use in the prediction of strong ground motions (Sommerville et al., 1999) can be considered as optimistic steps towards the particular problem. Nevertheless, the number of such studies is still relatively small and do not assure the identification of systematic characteristics in the slip patterns. Especially in Greece, studies regarding the earthquake source processes are extremely limited (to our knowledge, the only relevant work is that of Meyer et al., 1998) considering the plethora of earthquakes. This can be partly attributed to the fact that only recently broadband data are available. It is our belief that the national broadband network, which is now in full operation by NOA, will greatly improve our understanding of the role of the earthquake source to the ground motions.

Acknowledgements

We would like to express our gratitude to our colleagues at the National Observatory of Athens and especially to Dr. N. Melis for providing the broadband data and useful information. We are also thankful to Dr. C. Kontoes for giving us valuable information regarding the interferometric data of the Athens earthquake. We also thank the two reviewers, Ruth Harris and

Jim Mori, who provided constructive comments that helped us to improve the manuscript.

This work was financed by the Science for Peace Project (SfP 972342 Seis-Albania) and by OASP of Greece (Projects 20246/ 2000 and 70/3/5484).

References

Anastasiadis, An., Demosthenous, M., Karakostas, Ch., Klimis, N., Lekidis, B., Margaris, B., Papaioannou, Ch., Papazachos, C., and N. Theodoulidis (1999). The Athens (Greece) earthquake of September 7, 1999: Preliminary report on strong motion data and structural response, http://www.itsak.gr/report.html

Antolik, M. S. (1996). New results from studies of three outstanding problems in local, regional and global seismology, *PhD Thesis*, University of California, Berkeley, 311 pp.

Bouckovalas, G. D., and G. P. Kouretzis (2001). Stiff soil amplification effects in the 7 September 1999 Athens (Greece) earthquake, *Soil Dynamics and Earthquake Engineering* **21,** 671-687.

Clayton, R. W., and R. A. Wiggins (1976). Source shape estimation and deconvolution of teleseismic body waves, *Geophys. J. R. Astron. Soc.* **47,** 151-177.

Dreger, D. (1994). Empirical Green's function study of the January 17, 1994 Northridge, California earthquake, *Geophys. Res. Lett.,* **21,** 2633-2636.

Gazetas, G. (2001). The 1999 Parnitha (Athens) earthquake: Soil effects on distribution of damage, *Lessons learned from recent strong earthquakes (edt. Atilla Ansal),* International Society of Soil Mechanics and Geotechnical engineering, 5-18.

Kaverina, A., Dreger, D. S., and E. Price (2002). The combined inversion of seismic and geodetic data for the source process of the 16 October,

1999 Mw7.1 Hector Mine, California, earthquake, *Bull. Seism. Soc. Am.* **92**, Special issue on the Hector Mine earthquake, 1266 - 1280.

Kontoes, C., Elias, P., Sykioti, O., Briole, P., Remy, D., Sachpazi, M., Veis, G., and I. Kotsis (2000). Displacement field and fault model for the September 7, 1999 Athens earthquake inferred from ERS2 satellite radar interferometry, *Geophys. Res. Let.* **27,** 3989-3992.

Louvari, E., and A. Kiratzi (2001). Source parameters of the 7 September 1999 Athens (Greece) earthquake based on teleseismic data, *Journal of the Balkan Geophys. Soc.* **4,** 51-60.

Marinos, P., Bouckovalas, G., Tsiambaos, G., Protonotarios, G., Sabatakakis, N., and collaborators (1999). Damage distribution in the western part of Athens after the 7-9-99 earthquake, *Newsletter of the European Center on Prevention and Forecasting of Earthquakes,* **3,** 37-39.

Meyer, B., Armijo, R., Massonnet, D., De Chabalier, J. B., Delacourt, C., Ruegg, J. C., Achache, J., and D. Papanastassiou (1998). Results from combining tectonic observations and SAR interferometry for the 1995 Grevena earthquake: a summary, *J. Geodynamics,* **26,** 255-259.

Mori, J., and S. Hartzell (1990). Source inversion of the 1988 Upland earthquake: Determination of a fault plane for a small event, *Bull. Seism. Soc. Am.* **80,** 278-295.

National Observatory of Athens (NOA), *http://www.gein.noa.gr/*

Okada, Y. (1985). Surface deformations due to shear and tensile faults in a half-space, *Bull. Seism. Soc. Am.* **75,** 1135-1154.

Papadimitriou, P., Kaviris, G., Voulgaris, N., Kassaras, I., Delibasis, N., and K. Makropoulos (2000). The September 7, 1999 Athens earthquake sequence recorded by the Cornet Network: preliminary results of source parameters determination of the mainshock, *Annal. Geolog. de Pays Hel.*, 1e Serie, T. XXXVIII, Fasc. B, 29–35.

Papadopoulos, G. A., Drakatos, G., Papanastassiou, D., Kalogeras, I., and G. Stavrakakis (2000). Preliminary results about the catastrophic earthquake of 7 September 1999 in Athens, Greece, *Seism. Res. Let.* **71,** 318 –329.

Papazachos, B. C., and C. Papazachou (1997). The earthquakes of Greece, *Ziti Publ. Co.,* 356 pp.

Papazachos, C. B., Karakostas, B. G., Karakaisis G. F., and Ch. A. Papaioannou (2001). The Athens 1999 mainshock (M_w=5.9) and the evolution of its aftershock sequence, *Proc. of the 9th Int. Conf. of the Geological Society of Greece*, September 2001, Athens, 1581-1586.

Pavlides, S. B., Papadopoulos, G., and A. Ganas (2002). The fault that caused the Athens September 1999, M_S=5.9 earthquake: Field observations, *Natural Hazards*, in press.

Roumelioti, Z., Kiratzi, A., Theodoulidis, N., Kalogeras, I., and G. Stavrakakis (2002). Rupture directivity during the September 7, 1999 (M_w 5.9) Athens earthquake inferred from forward modeling of strong ground motion, *Pageoph*, in press.

Somerville, P., Irikura, K., Graves, R., Sawada, S., Wald, D., Abrahamson, N., Iwasaki, Y., Kagawa, Smith, N., and A.Kowada (1999). Characterizing

crustal earthquake slip models for the prediction of strong ground motion, *Seism. Res. Let.*, **70,** 59-80.

Tselentis, G., and J. Zahradnik (2000). The Athens earthquake of 7 September 1999, *Bull. Seism. Soc. Am.* **90**, 1143-1160.

Wells, D. L., and K. J. Coppersmith (1994). New empirical relationships among magnitude, rupture length, rupture width, rupture area and surface displacement, *Bull. Seism. Soc. Am.* **84,** 974-1002.

Zahradnik, J. (2002). Focal mechanism of the Athens 1999 earthquake by ASPO method, *Tectonophysics,* submitted.

Zahradnik, J., and G.-A. Tselentis (2002). Modeling strong-motion accelerograms by PEXT method, application to the Athens 1999 earthquake, *Bull. Seism. Soc. Am.,* submitted.

Figure captions

Figure 1: Map showing the locations of the broadband stations used in the present study, with respect to the epicenter of the Athens earthquake.

Figure 2: North-South and East-West component displacement seismograms, corresponding to three different regional paths, are compared for the Athens mainshock and the selected aftershock (EGF).

Figure 3: Source time functions at station APE derived from the deconvolution of the EW (upper part) and NS (middle part) EGF components from the mainshock are compared to their stack (lower part).

Figure 4: Far-field source time functions obtained by deconvolving the broadband waveforms of an M_w 4.5 aftershock from the corresponding waveforms of the Athens mainshock. The STF's are normalized to unit area. The name and azimuth of each station is noted on the top right.

Figure 5: Slip distribution during the Athens earthquake obtained from the STF inversion using a rupture velocity of 2.7 Km/sec and a rise time of 0.4 sec. Contours are for 10 cm of slip. Star denotes the hypocentral location and dotted frames the areas of maximum concentration of slip.

Figure 6: a) Coseismic interferogram estimated by Kontoes et al. (2000). **b)** Synthetic surface displacement field for the Athens earthquake obtained using the slip distribution model of Figure 5. **c)** Synthetic surface displacement field for the Athens earthquake produced by the shallower slip patch depicted in Figure 5. **d)** Synthetic surface displacement field for the Athens earthquake produced by the deep slip patch of Figure 5.

Table 1 Source parameters for the Athens mainshock and the aftershock used as empirical Green's function. Results from several researchers are listed for the mainshock.

Event	Date	Time	Latitude	Longitude	Depth	**M**	Mo	Strike/Dip/Rake	Reference
	DD/MM/YY	h:m:s	(°N)	(°E)	(Km)		$*10^{17}$Ntm	(°)	
Main	07/09/99	11:56:51	38.08	23.58	16.8	5.9	-	113/39/-90	Papadopoulos et al. (2000)
			38.13	23.55	9.0		7.8	123/55/-84	USGS
			38.02	23.71	15.0		12.0	114/45/-73	Harvard
			38.11	23.57	8.0		17.0	105/55/-80	Papadimitriou et al. (2000)
			38.06	23.57	14.5		-	-	Papazachos et al. (2001)
			-	-	10.0		9.22	115/57/-80	Louvari and Kiratzi (2001)
			-	-	-		-	112/61/-84	Zahradnik (2002)
eGf	7/9/99	20:32:27	38.12	23.63					

22

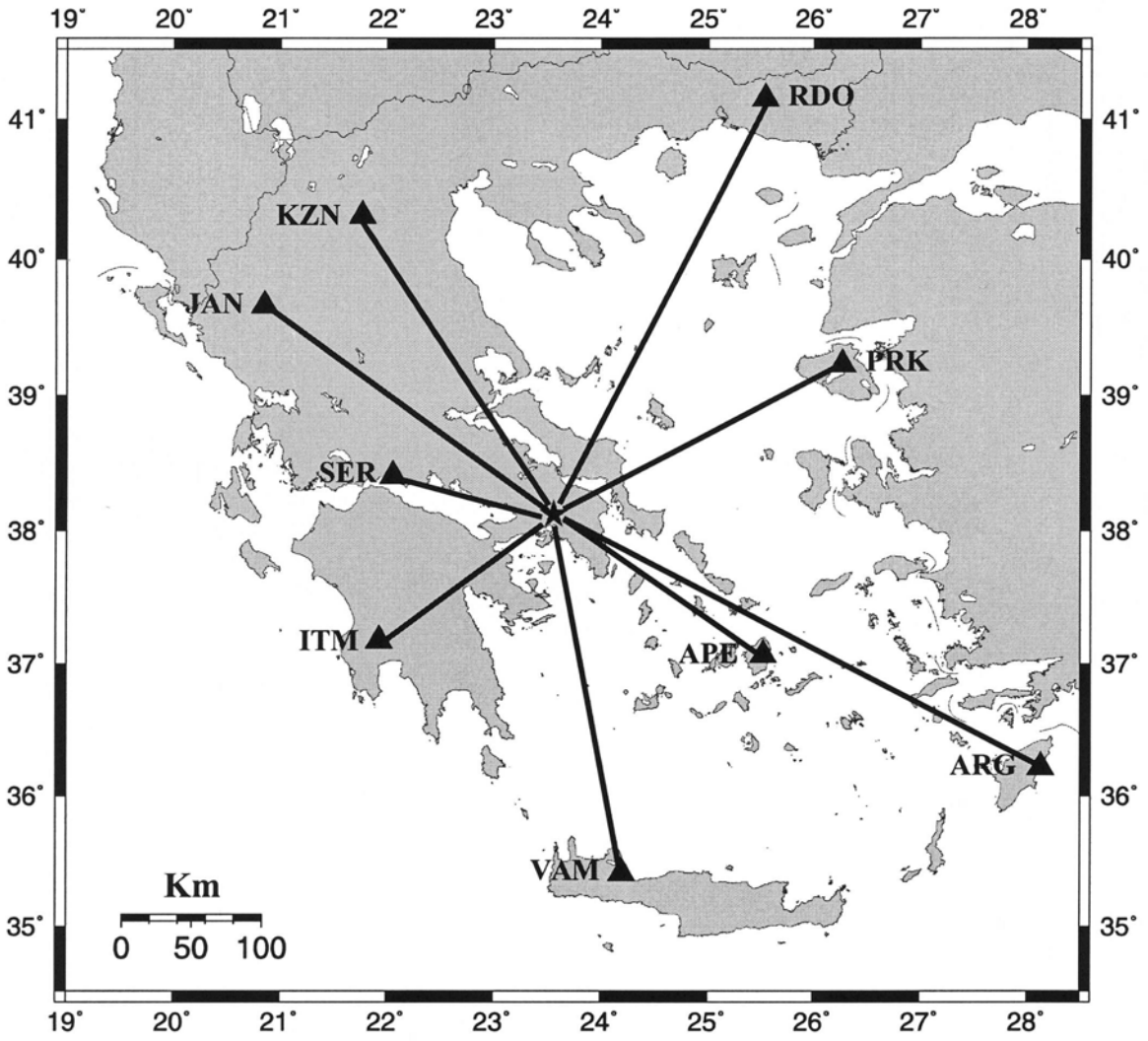
19°
20°
21°
22°
23°
24°
25°
26°
27°
28°
41°
40°
39°
38°
37°
36°
35°
RDO
KZN
JAN
PRK
SER
ITM
APE
ARG
VAM
Km
0 50 100

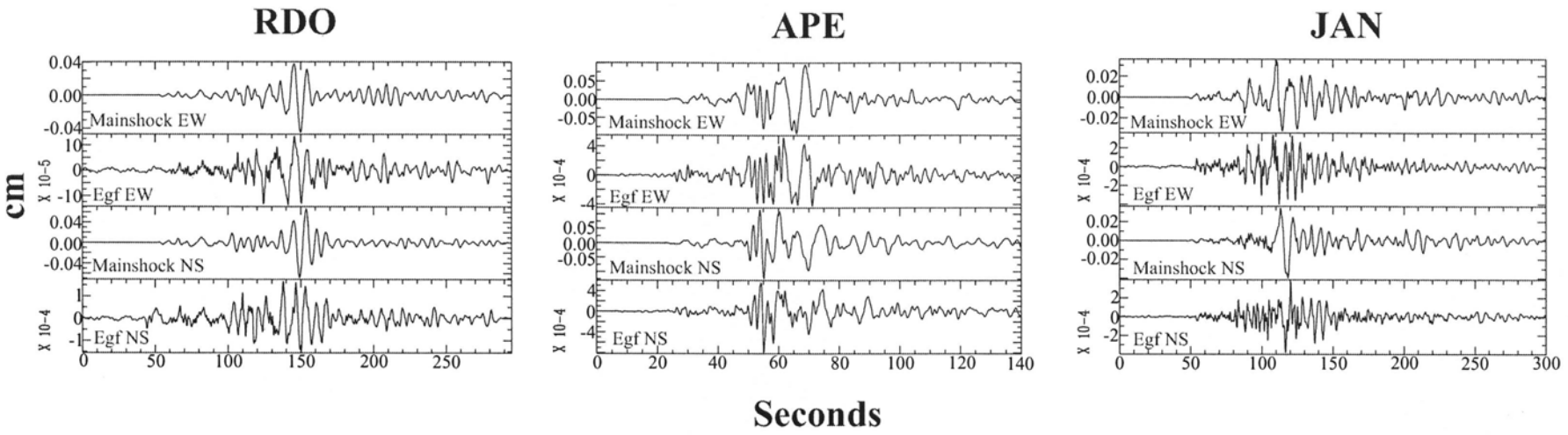
RDO
APE
JAN
cm
Mainshock EW
Egf EW
Mainshock NS
Egf NS
X 10-5
X 10-4
Seconds

Figure 2

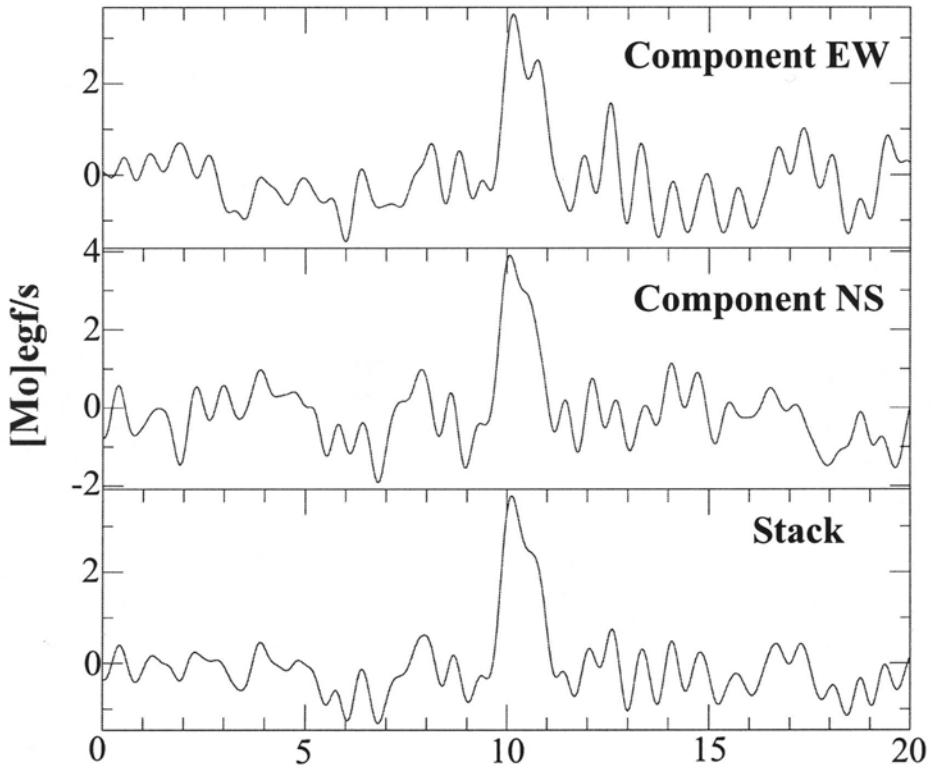

Figure 3

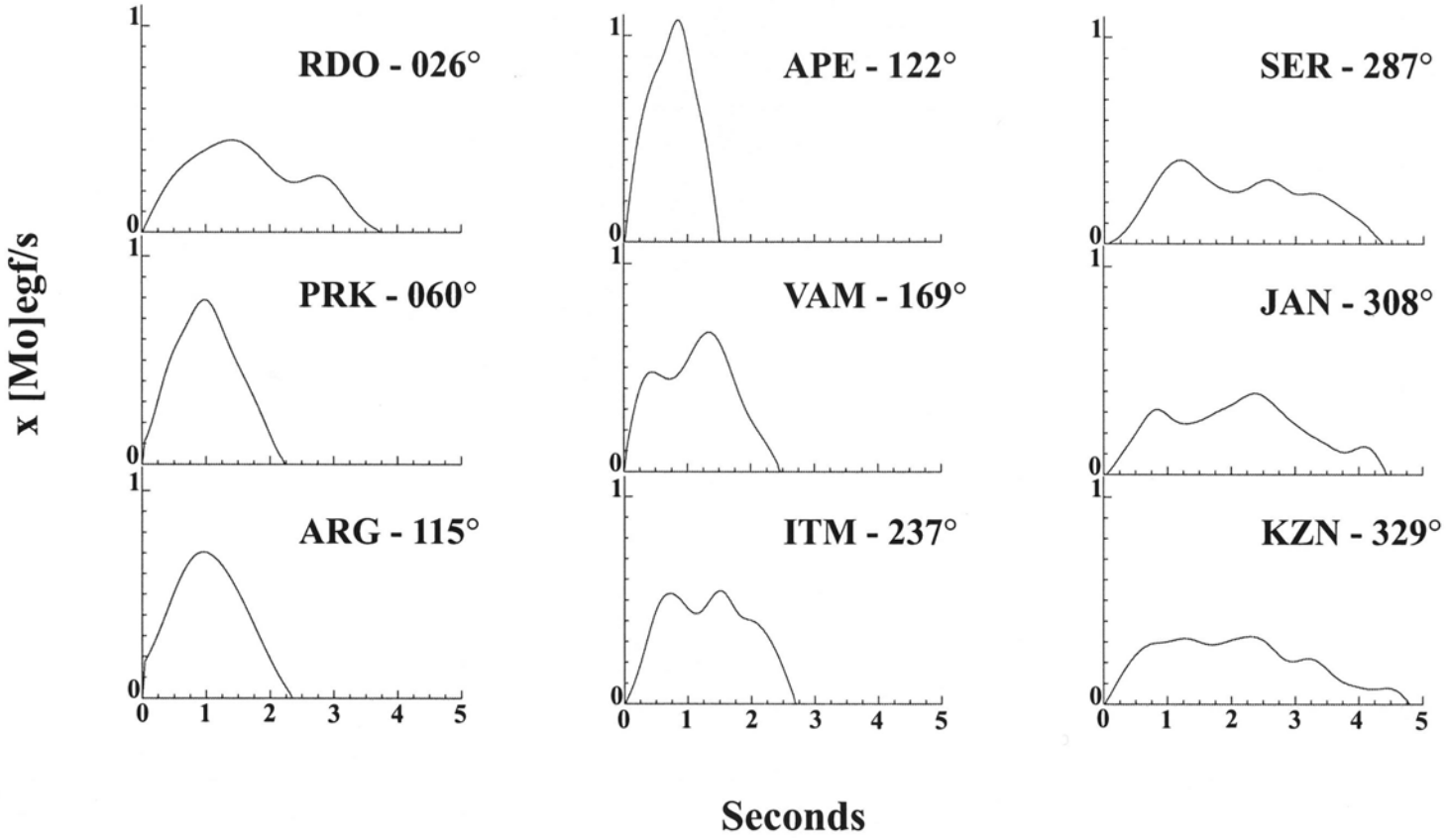
RDO - 026°
APE - 122°
SER - 287°
PRK - 060°
VAM - 169°
JAN - 308°
ARG - 115°
ITM - 237°
KZN - 329°
x [Mo]egf/s
Seconds

Figure 4

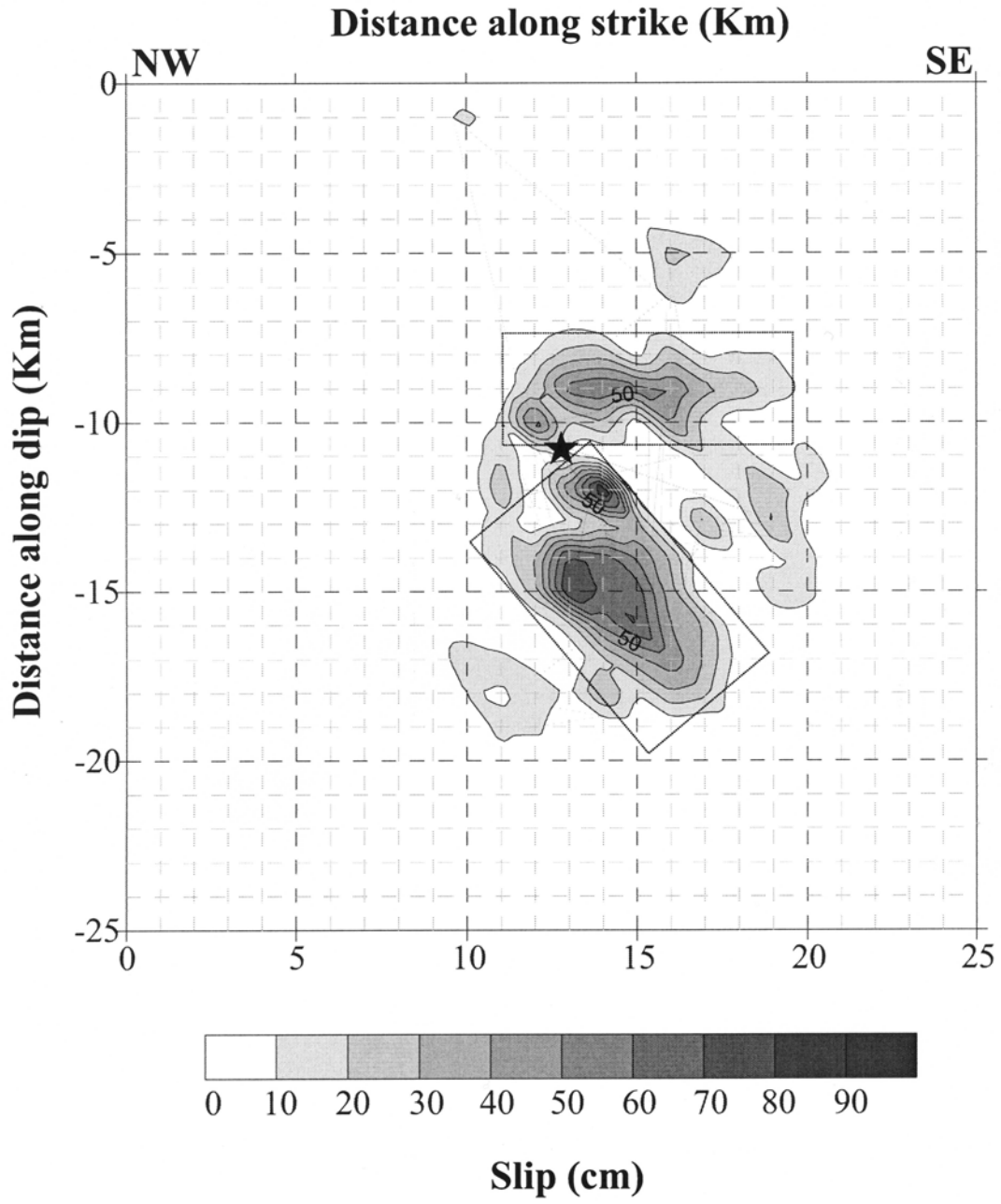
Distance along strike (Km)
NW
SE
0
-5
-10
-15
-20
-25
Distance along dip (Km)
50
50
50
0
5
10
15
20
25
0 10 20 30 40 50 60 70 80 90
Slip (cm)

Figure 5

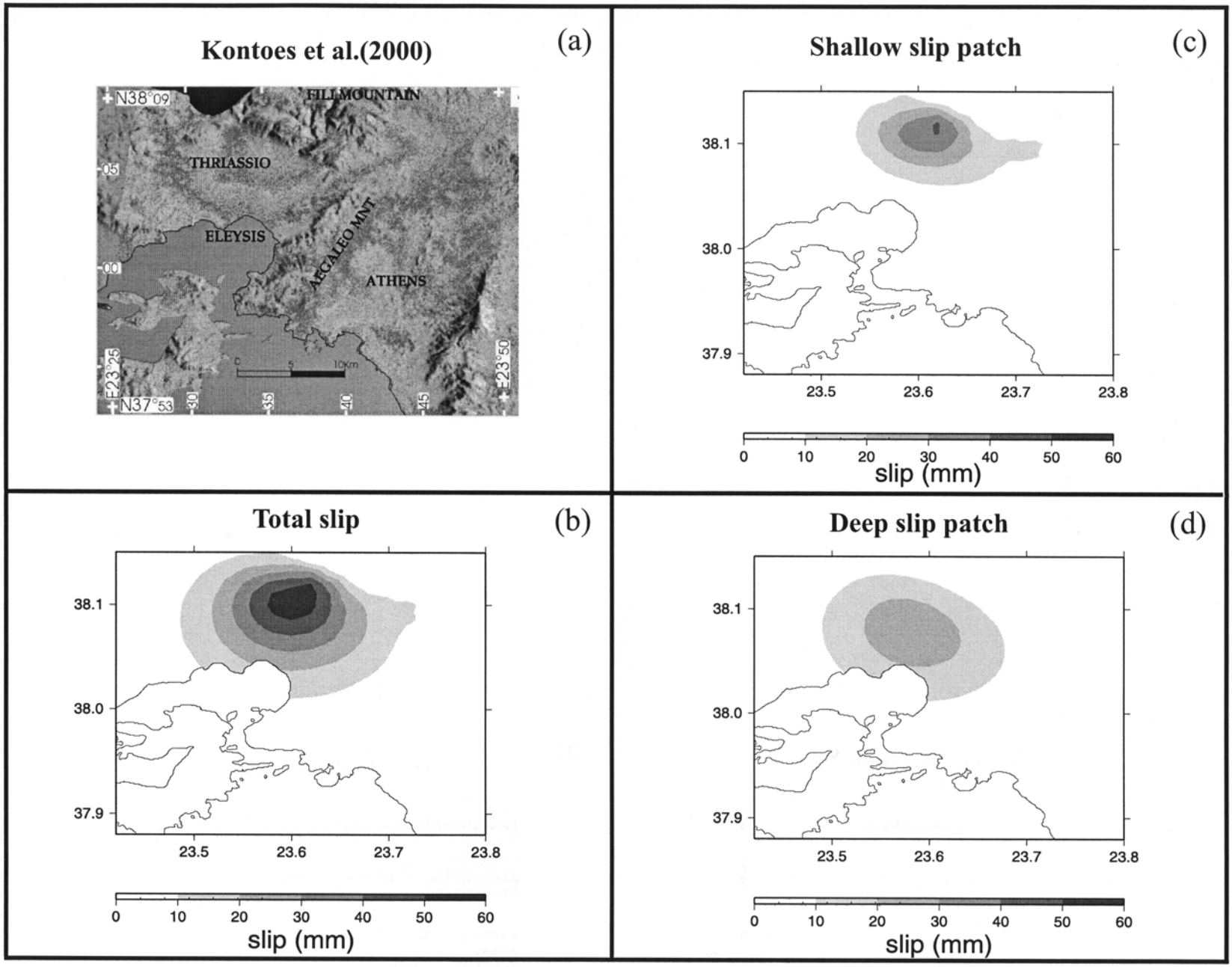
Kontoes et al.(2000)
(a)
N38°09
FILLMOUNTAIN
THRIASSIO
05
ELEYSIS
00
AEGALEO MNT
ATHENS
E23°25
E23°50
N37°53
30
35
40
45
0
5
10Km
Shallow slip patch
(c)
38.1
38.0
37.9
23.5
23.6
23.7
23.8
0
10
20
30
40
50
60
slip (mm)
Total slip
(b)
38.1
38.0
37.9
23.5
23.6
23.7
23.8
0
10
20
30
40
50
60
slip (mm)
Deep slip patch
(d)
38.1
38.0
37.9
23.5
23.6
23.7
23.8
0
10
20
30
40
50
60
slip (mm)

Figure 6